

# You Can Mask More For Extremely Low-Bitrate Image Compression

Anqi Li<sup>1,2†</sup> · Feng Li<sup>3†</sup> · Jiaxin Han<sup>1,2</sup> · Huihui Bai<sup>1,2\*</sup> · Runmin Cong<sup>4</sup> ·  
Chunjie Zhang<sup>1,2</sup> · Meng Wang<sup>3</sup> · Weisi Lin<sup>5</sup> · Yao Zhao<sup>1,2</sup>

Received: date / Accepted: date

**Abstract** Learned image compression (LIC) methods have experienced significant progress during recent years. However, these methods are primarily dedicated to optimizing the rate-distortion (R-D) performance at medium and high bitrates ( $> 0.1$  bits per pixel (bpp)), while research on extremely low bitrates is limited. Besides, existing methods fail to explicitly explore the image structure and texture components crucial for image compression, treating them equally alongside uninformative components in networks. This can cause severe perceptual quality degradation, especially under low-bitrate scenarios. In this work, inspired by the success of pre-trained masked autoencoders (MAE) in many downstream tasks, we propose to rethink its mask sampling strategy from structure and texture perspectives for high redundancy reduction and discriminative feature representation, further unleashing the potential of LIC methods.

Therefore, we present a dual-adaptive masking approach (DA-Mask) that samples visible patches based on the structure and texture distributions of original images. We combine DA-Mask and pre-trained MAE in masked image modeling (MIM) as an initial compressor that abstracts informative semantic context and texture representations. Such a pipeline can well cooperate with LIC networks to achieve further secondary compression while preserving promising reconstruction quality. Consequently, we propose a simple yet effective masked compression model (MCM), the first framework that unifies MIM and LIC end-to-end for extremely low-bitrate image compression. Extensive experiments have demonstrated that our approach outperforms recent state-of-the-art methods in R-D performance, visual quality, and downstream applications, at very low bitrates. Our code is available at <https://github.com/lianqi1008/MCM.git>.

**Keywords** Extremely Low-Bitrate Image Compression · Masked Compression Model · Dual-Adaptive Masking

## 1 Introduction

Image compression is a fundamental and crucial technique in image processing, with the goal of signal redundancy removal, to pursue efficient storage and transmission while maintaining high perceptual quality, which is ubiquitous in real-world applications. Classical compression standards such as JPEG [51], JPEG2000 [50], BPG [6], VVC [8] adopt the sequential paradigm of “transformation, quantization, and entropy coding”, where each is separately optimized with hand-crafted rules, making it hard to be adapted to diverse image content.

---

Anqi Li: [lianqi@bjtu.edu.cn](mailto:lianqi@bjtu.edu.cn)  
Feng Li: [fengli@hfut.edu.cn](mailto:fengli@hfut.edu.cn)  
Jiaxin Han: [hanjiaxin@bjtu.edu.cn](mailto:hanjiaxin@bjtu.edu.cn)  
Huihui Bai: [hbbai@bjtu.edu.cn](mailto:hbbai@bjtu.edu.cn)  
Runmin Cong: [rmcong@sdu.edu.cn](mailto:rmcong@sdu.edu.cn)  
Chunjie Zhang: [ivazhangchunjie@gmail.com](mailto:ivazhangchunjie@gmail.com)  
Meng Wang: [eric.mengwang@gmail.com](mailto:eric.mengwang@gmail.com)  
Weisi Lin: [wslin@ntu.edu.sg](mailto:wslin@ntu.edu.sg)  
Yao Zhao: [yzhao@bjtu.edu.cn](mailto:yzhao@bjtu.edu.cn)

<sup>1</sup> Institute of Information Science, Beijing Jiaotong University

<sup>2</sup> Beijing Key Laboratory of Advanced Information Science and Network Technology

<sup>3</sup> School of Computer Science and Engineering, Hefei University of Technology

<sup>4</sup> School of Control Science and Engineering, Shandong University

<sup>5</sup> School of Computer Science and Engineering, Nanyang Technological University

† Equal contribution.

\* Corresponding author.

During recent years, deep learning-based approaches [2, 4, 41, 42, 57] have dominated the image compression field due to their end-to-end optimization. Typical learned image compression (LIC) methods follow the variational autoencoder (VAE) design in [4] and construct different autoencoder architectures [10, 30, 36, 17] or entropy models [41, 34, 44] to optimize for rate-distortion (R-D) performance measured by the Peak Signal-to-Noise Ratio (PSNR) and Multi-Scale-Structural Similarity Index Measure (MS-SSIM). These methods prioritize improving such metric scores with more competitive bitrates as traditional codecs (*i.e.* BPG and VVC), while the compression at very low bitrates ( $\leq 0.1$  bpp) still lacks sufficient research attention. Agustsson *et al.* [48] present a generative adversarial network (GAN)-based compression framework that achieves dramatic bitrate savings. The results tend to maintain the high-level semantics but with significant deviated details of original inputs. Besides, the structure and texture components of an image have different tolerance for compression distortion, especially at low bitrates. Nevertheless, both traditional and most existing LIC methods consider all image components equally during their compression process. Due to the lack of explicit exploration of such two components, directly applying these methods to extremely low-bitrate compression scenarios can cause serious degradation of reconstruction quality. Several methods [14, 13] introduce conceptual compression which characterizes visual structure and texture into deep compact representations for individual compression but show limited perceptual quality at low bitrates. How to adapt both two components to achieve extremely low-bitrate compression while preserving high-quality reconstruction is still a serious challenge.

Recently, masked autoencoder (MAE) [23] has exhibited great success on various computer vision tasks. Its superiority can be attributed to the masked sampling and self-supervised pre-training framework, which masks random patches from the input image and only operates on the remaining visible patches to reconstruct masked ones. MAE demonstrates that masking a high portion of patches can effectively reduce data redundancy, thus contributing to efficient learning. Therefore, it is natural for us to consider whether can combine MAE and LIC to achieve extremely low-bitrate compression. However, simply implementing such random masking in image compression is sub-optimal, as it may discard some important texture or structure information and instead preserve some meaningless patches, resulting in less discriminative representation and inaccurate reconstruction.

Based on the above analysis, in this paper, we propose the masked compression model (MCM) which borrows the idea of MAE to unleash the potential of LIC at low bitrate conditions. Our MCM stems from the fact that the appearance of visual objects is depicted through structures and textures, and the complexity of such two components heavily affects visual analysis and content synthesis. Therefore, we first present a dual-adaptive masking (DA-Mask) approach, which performs patch sampling based on structure and texture distributions. To be specific, we simultaneously quantify the edge information and semantic context to model the texture and structure complexity of all patches in an image. Then, we adopt probability sampling to select visible patches by estimating the categorical distribution over all patches conditioned on both complexity scores. In this way, compared to the random sampling strategy in MAE, our DA-Mask can adaptively sample more informative patches that are conducive to image reconstruction while achieving effective redundancy removal. Moreover, by incorporating the advantages of DA-Mask and pre-trained MAE into masked image modeling (MIM), we enable an initial compressor to abstract meaningful semantic context and texture representation. Subsequently, operating on the learned representations, a simple yet effective deep codec is utilized to conduct further secondary compression and high-quality image reconstruction. Therefore, our MCM can be seen as an end-to-end two-stage framework that unifies MIM and LIC for extremely low-bitrate compression. Extensive experimental results demonstrate the effectiveness of our method which outperforms the existing state-of-the-art methods in perceptual quality at very low bitrates. We also combine MCM with existing segmentation and detection backbones to evaluate the performance of MCM on downstream tasks and our MCM achieves better results than various LIC methods. The contributions of this paper are summarized as follows.

- We propose a novel masked compression model (MCM) for extremely low-bitrate compression. To the best of our knowledge, this is the first framework that generalizes the self-supervised pre-trained MAE to LIC.
- We propose a dual-adaptive masking (DA-Mask) approach based on structure and texture distributions, which can adaptively sample more informative patches while achieving effective redundancy removal.
- We combine DA-Mask and pre-trained MAE into masked image modeling as an initial compressor to abstract meaningful semantic context and texture

- representations. Such a pipeline can well cooperate with LIC networks to achieve two-step compression.
- Extensive experiments demonstrate the superiority of the proposed method against recent state-of-the-art LIC methods in visual quality at very low bitrates. MCM also outperforms previous methods on downstream tasks.

## 2 Related Work

### 2.1 Learned Image Compression

Since Ballé *et al.* [3] first propose the pioneering end-to-end image compression method using convolutional neural network (CNN), deep learning models have been widely used in image compression and demonstrated remarkable achievement. [4] introduces a scale hyperprior into [3] to capture spatial dependencies in the latent representation, which provides a general variational autoencoder (VAE) compression pipeline, inspiring later research. Minner *et al.* [41] combine an autoregressive model with the hyperprior in a joint framework to predict latents from their causal context. Lee *et al.* [34] exploit bit-consuming and bit-free contexts to build a context-adaptive entropy model that more accurately estimates the distribution of each latent representation. Cheng *et al.* [17] leverage discretized Gaussian mixture likelihoods-based entropy model and attention modules to enhance the R-D performance. Apart from these CNN-based models, motivated by the outstanding performance in a broad range of computer vision tasks [32, 11, 16, 56, 39], some methods have also investigated the potential of vision transformers in learned image compression (LIC). Bai *et al.* [1] integrate LIC with ViT-based image analysis [32] to exploit the synergy effect of these two tasks. Motivated by the window attention in Swin Transformer [39], Chen *et al.* [58] present window attention-based symmetrical transformer (STF) framework which shows better R-D performance than previous CNN-based methods. In [44], a transformer-based entropy model is proposed to improve LIC by accuracy probability distribution estimation.

Beyond the above VAE style methods, there are also some other attempts for LIC. For example, Xie *et al.* [53] propose an enhanced invertible encoding network based on invertible neural networks (INN) [20] to largely capture the lost information for better compression. Chang *et al.* [14] present conceptual compression, which decomposes the image contents into structural and textural layers and separately compresses each of them, resulting in high reconstruction quality at very low bitrates. [13]

introduces consistency-contrast learning in conceptual compression to align the structure of texture representation space and source image space. [48, 18] exploit the image generation capabilities of generative adversarial networks (GAN) to improve the perceptual quality of low-bitrate compressed images. Different from these methods, this work is inspired by the mask sampling and pre-training schemes in MAE and combines them with LIC to target effective extremely low-bitrate compression.

### 2.2 Masked Image Modeling

Masked image modeling (MIM) can be derived from masked language modeling in natural language processing (NLP) [19, 45, 46, 9], which adopts self-supervised pre-training paradigm to learn representations from unlabeled datasets by predicting the randomly masked patches in an image and then fine-tuning for specific downstream tasks. The representative method of MIM is masked autoencoder (MAE) [23] which applies a standard ViT [32] as the encoder to operate on reserved visible patches and then reconstructs the missing patches with a lightweight decoder. In [54], Xie *et al.* propose to regress the raw pixels of masked patches with  $\ell_1$  loss, which performs comparably to patch classification approaches [32, 39, 5]. CMAE [27] imposes contrastive learning into MAE to improve the representation of MIM. GreenMAE [26] extends the asymmetric encoder-decoder architecture of MAE to hierarchical vision transformers to better model hierarchical representations and local inductive bias. MCMAE [22] introduces hybrid convolution-transformer architectures with masked convolution for mask autoencoding.

In addition to the exploration of MIM on high-level vision tasks, there are also some works that have been proposed to study the effectiveness of MIM for image generation. Chang *et al.* [12] propose a masked generative image transformer (MaskGIT) that learns to generate all tokens of an image from randomly masked tokens. MAGE [37] unifies generative training and self-supervised representation learning in a single token-based MIM framework for class-unconditional image generation. Lezama *et al.* [35] propose a token-critic transformer to select which tokens should be accepted or resampled. Duan *et al.* [21] develop MAE pre-training based on an efficient window attention-based transformer to tackle image processing tasks such as image denoising, deblurring, and deraining *et al.*. However, the significance of MIM on image compression has not been researched. In this work, we show that the pre-trained MAE can also be seen

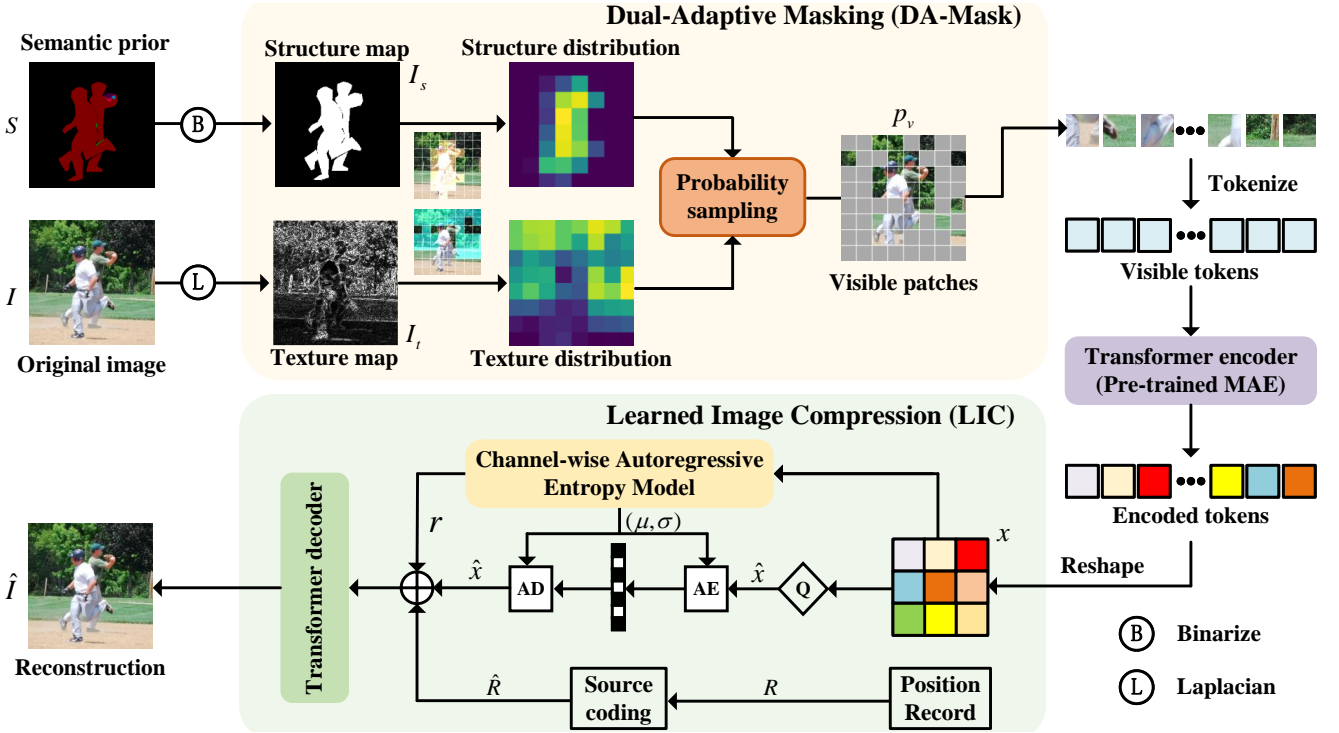


Fig. 1: The overall framework of our masked compression model (MCM) which unifies pre-trained MAE [23]-based MIM and LIC for extremely low-bitrate image compression. We replace the random sampling in MAE with our dual-adaptive masking approach (DA-Mask). “Q”, “AE”, and “AD” denote quantization, arithmetic encoding, and arithmetic decoding, respectively.

as an initial compressor that can well cooperate with LIC architectures. Besides, we propose a dual-adaptive masking approach that samples visible patches based on the structure and texture distributions of original images, thus learning more informative representations than the above random sampling strategy in MIM.

### 3 Proposed Method

#### 3.1 Problem Formulation

The goal of our proposed masked compression model (MCM) is to provide a new paradigm for extremely low-bitrate compression. As illustrated in Fig. 1, MCM is a two-stage framework that unifies pre-trained MAE [23]-based MIM and LIC in an end-to-end manner. Given an image  $I$  and its corresponding semantic prior  $S$ , in the first stage, a dual-adaptive masking approach is utilized to perform adaptive patch sampling based on the structure and texture distributions of  $I$ . Here, the texture distribution of each patch is calculated over all patches according to the Laplacian-detected texture map  $I_t$  and the structure distribution is obtained from the structure map  $I_s$ , *i.e.* the binary

version of the semantic map  $S$ . Thus, we can obtain texture- and structure-sensitive patches  $p_t$  and  $p_s$  which highly describe the appearance of visual objects. Then, probability sampling is utilized to decide the final candidate patches conditioned on  $p_t$  and  $p_s$ . The main process of DA-Mask is formulated as:

$$p_v = \mathcal{M}(I, S) \quad (1)$$

where  $\mathcal{M}(\cdot)$  denotes the DA-Mask operation to obtain the visual patches  $p_v$  in  $I$ .

After that, receiving the visible tokens by the tokenization on the visible patches  $p_v$ , similar to MAE [23], we also apply a pre-trained standard ViT [32] as the encoder  $E$  to learn latent representations, resulting in encoded tokens  $x$  of  $p_v$ :

$$x = E(p_v) \quad (2)$$

Therefore, equipped with DA-Mask, our MCM can achieve initial compression from structure and texture perspectives, enabling to abstract more informative representations for later LIC.

In the second stage, we do not design specific architecture and only build the LIC module upon the channel-wise auto-regressive entropy model [42].

Especially, the encoded tokens  $x$  are first reshaped as the input of LIC for quantization  $Q$ , arithmetic encoding  $AE$ , arithmetic decoding  $AD$ , and entropy model. Besides, different from existing LIC methods [42], considering that the positional information of tokens is critical to locate the mask tokens attending in an image, we transmit the position record of visible patches  $R$  with a source coding approach (Huffman coding [28] in this work) to support for mask prediction. Finally, a lightweight transformer decoder  $D$  is utilized to reconstruct the decompressed image  $\hat{I}$ . The main process of LIC stage can be formulated as:

$$\begin{aligned} \hat{x} &= Q(x) \\ \hat{R} &= Huffman(R) \\ \hat{I} &= D(\hat{x}, r, \hat{R}) \end{aligned} \quad (3)$$

where *Huffman* denotes Huffman coding operations.  $\hat{R}$  is the decoded position record of  $R$ .  $r$  is the residual produced by the entropy model to reduce the quantization errors  $x - \hat{x}$ .

### 3.2 Dual-Adaptive Masking

Since different patches contain different information, simply implementing such a random mask sampling as existing MIM methods [23, 12, 37] may preserve some meaningless patches and discard some important texture or structure information that is important for visual understanding, resulting in misleading reconstruction. Therefore, we propose the dual-adaptive masking (DA-Mask) approach to adaptively sample informative patches that are conducive to image reconstruction while achieving effective redundancy removal. As shown in Fig. 1, DA-Mask contains two branches that model the texture and structure complexity of all patches to guide later probability sampling.

**Texture Complexity Modeling.** Considering that the edge prior reveals the sharpness of local regions in an image and is high-related to texture details recovery, we quantify the edge information of each patch to measure the texture complexity. To be specific, given an RGB image  $I$  with the spatial size of  $H \times W$ , the texture map  $I_t$  is obtained by the edge information extraction on  $I$  using a 2nd-order Laplacian differential operator which has been demonstrated to have a more stable location ability, better sharpness, and more robust to noise [49]

$$I_g = RGB2Gray(I) \quad (4)$$

$$I_t = \frac{\partial^2 I_g}{\partial x^2} + \frac{\partial^2 I_g}{\partial y^2}, I_t \in \mathbb{R}^{1 \times H \times W} \quad (5)$$

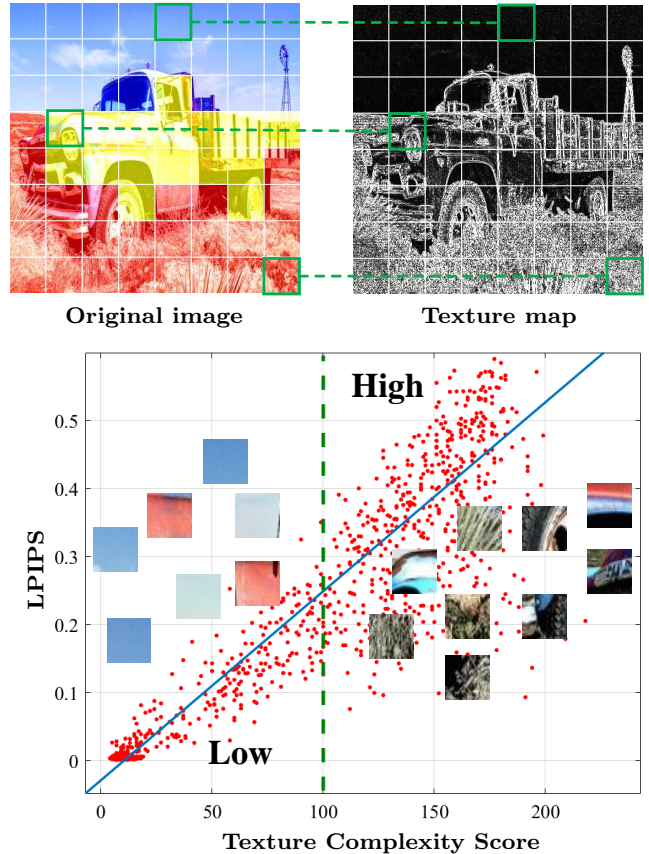


Fig. 2: The correlation between texture complexity and reconstruction quality. Top: the original image and detected texture map by 2nd-order Laplacian differential operator. Bottom: the LPIPS of the image patches with different texture complexity scores.

where  $I_g$  is the grayscale version of  $I$  produced by the convert function *RGB2Gray*. We then split both  $I$  and  $I_t$  into serial non-overlapped patches, denoted as  $p \in \mathbb{R}^L$  and  $p_t \in \mathbb{R}^L$ , where  $L = \frac{H}{N} \times \frac{W}{N}$  represents the number of patches with the spatial size of  $N \times N$ . The texture complexity score of a certain image patch is calculated by absolutely summing the absolute values of all elements inside its corresponding texture patch.

$$Score_t^l = \sum_{i=1}^N \sum_{j=1}^N |p_t^l(i, j)| \quad (6)$$

where  $Score_t^l$  is the score of the  $l$ -th patch  $p^l$ .  $(i, j)$  denotes the position of the patch. In this work, we set the patch size  $N \times N$  as  $16 \times 16$ . Therefore, for  $L$  patches, we can get all the scores  $(Score_t^1, Score_t^2, \dots, Score_t^L)$ .

The correlation between texture complexity and reconstruction quality is illustrated in Fig. 2. We adopt BPG [6] to compress them and rank their performance using Learned Perceptual Image Patch Similarity (LPIPS). It can be observed that the

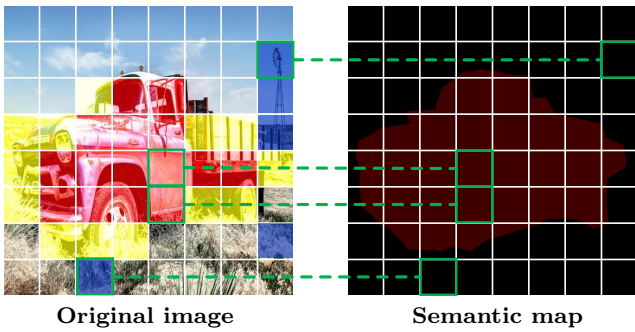


Fig. 3: The patch-wise correspondences between the original image and semantic map.

patches with low texture complexity tend to have low LPIPS (better), while the patches with high LPIPS (worse) contain more textures. Based on this observation, we can conclude that: 1) The patch involving large texture complexity is hard to be reconstructed after compression; 2) Masking a portion of very smooth patches yet preserving complex ones can effectively reduce the pixel redundancy and alleviate the prediction burden on local textures.

**Structure Complexity Modeling.** Though the texture-based patch sampling strategy can help to learn texture-aware representations, as shown in Fig. 3, it can lead to the network over-emphasizing the background regions with complex textures (blue patches) and ignoring some important smooth parts (red patches) of visual objects. In fact, it is crucial to capture the semantic context of objects for both visual analysis and image synthesis tasks. To address this problem, we propose to model the structure complexity as an additional guidance for more informative patch sampling.

Specifically, for the input image  $I$ , we adopt its semantic map  $S$  as prior to generate a structure map  $I_s$  by binary operation. Similar to the texture-based strategy, besides the image patch  $p$ , we also split  $I_s$  into multiple  $N \times N$  non-overlapped patches, resulting in  $p_s$ . Then, we measure the structure complexity by directly summing all the internal elements

$$Score_s^l = \sum_{i=1}^N \sum_{j=1}^N p_s^l(i, j) \quad (7)$$

where  $Score_s^l$  denotes the semantic score of the  $l$ -th patch. Correspondingly, for total  $L$  patches of  $I$ , we can obtain the scores  $(Score_1^l, Score_2^l, \dots, Score_L^l)$ . In this way, we can effectively capture the semantic richness of each patch that describes the global structure of visual objects, which helps DA-Mask perform semantic-oriented masking.

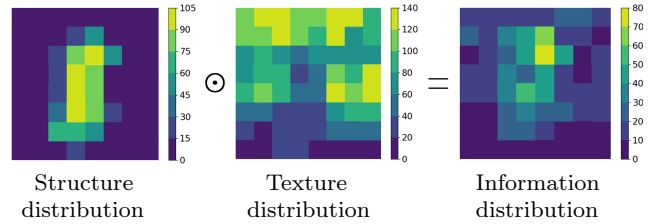


Fig. 4: The visualization of structure, texture, and information distributions based on corresponding complexity scores and information capacity.

**Probability Sampling.** As mentioned above, both the texture and structure complexity of each patch are important for informative representation learning and content recovery. Therefore, in DA-Mask, probability sampling is introduced to select visible patches based on the texture and structure distributions of input image  $I$ . As shown in Fig. 4, we generalize the texture and structure complexity scores of all the patches to represent the overall texture and structure distributions respectively. After that, we conduct patch-wise multiply on the texture and structure complexity scores as the information capacity of each patch to reveal which one is beneficial for discriminative learning or meaningless.

$$Inf_l = Score_s^l \odot Score_t^l \quad (8)$$

where  $Inf_l$  denotes the information capacity of the  $l$ -th patch. A toy example of resulted information distribution is shown in Fig. 4. We then estimate the categorical distribution  $Cat$  over all image patches according to the softmax normalized  $Inf_l$ .

$$Cat(\alpha_1, \alpha_2, \dots, \alpha_L) = Softmax(Inf_l), \sum_l \alpha_l = 1 \quad (9)$$

where  $(\alpha_1, \alpha_2, \dots, \alpha_L)$  denote the normalized parameters of  $(Inf_1, Inf_2, \dots, Inf_L)$ . Supposing the masking ratio is  $\rho \in (0, 1)$ , the number of masked patches is equal to  $L \times \rho$ . Gumbel-softmax trick [29] is leveraged to determine the visible patch set  $p_v$  which contains  $L \times (1 - \rho)$  sampled patches. In summary, based on the above analysis, our DA-Mask enables sampling the patches that can well balance the local texture and structural semantics and is prone to mask the patches with less information, resulting in effective redundancy removal.

### 3.3 Transformer Encoder/Decoder

Following [23], as shown in Fig. 5, for the encoder, we use the standard ViT with relative position

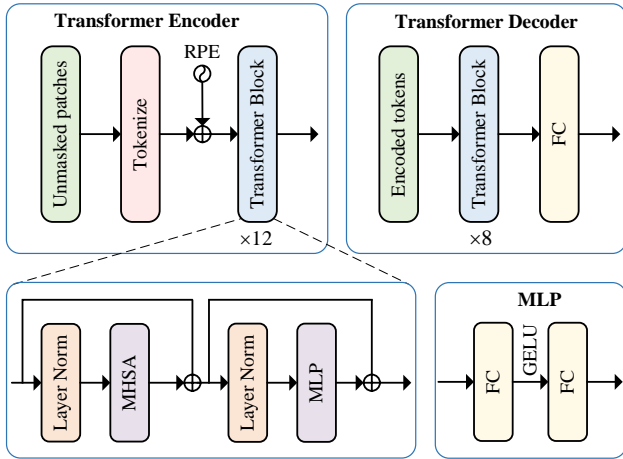


Fig. 5: Architectures of the transformer encoder and transformer decoder in our MCM. Here, “RPE” and “FC” denote relative position embedding and full-connected layer.

embedding as the backbone which contains cascaded 12 transformer blocks. Each block consists of a multi-head self-attention (MHSA) and a multi-layer perceptron (MLP) with layer normalization (Layer Norm). The transformer decoder is more lightweight, which uses 8 transformer blocks and an additional full-connected layer followed by reshape operation to reconstruct the final image.

### 3.4 Loss Function

As shown in Fig.1, our MCM unifies pre-trained MAE [23]-based MIM and LIC for extremely low-bitrate image compression. Therefore, it involves two training stages, *i.e.*, the pre-training on our transformer encoder in MIM to learn meaningful representation, and the joint optimization of overall MCM. The former is trained on ImageNet-1K dataset using MSE as the loss function to constrain the original image  $I$  and reconstructed image  $\hat{I}$ . In the second stage, the LIC module receives initialized features by the pre-trained weights and then is jointly optimized with the MIM using Rate-Distortion (R-D) loss  $\mathcal{L}$ :

$$\mathcal{L} = \mathcal{R} + \lambda \mathcal{D}(I, \hat{I}), \quad (10)$$

where  $\lambda$  is a Lagrangian multiplier factor to control the R-D trade-off.  $\mathcal{R}$  denotes the bitrates estimated by the entropy model. The distortion loss  $\mathcal{D}$  is a composited function that contains  $L_1$ , SSIM [52], and VGG [31] losses, denoted by

$$\mathcal{D} = \lambda_1 \|I - \hat{I}\|_1 + \lambda_2 SSIM(I, \hat{I}) + \lambda_3 VGG(I, \hat{I}), \quad (11)$$

where  $\lambda_1$ ,  $\lambda_2$  and  $\lambda_3$  are hyper-parameters that balance the three components. In this work, we set them to 10, 0.25, and 0.1 respectively.

## 4 Experiments

### 4.1 Experimental Setup

We use MS COCO [38] and CelebAMask-HQ [33] to evaluate the performance of our MCM. Here, MS COCO contains 82783 images for training and 40504 images for testing. We randomly select 200 images from the testing set for performance evaluation. CelebAMask-HQ contains 30000 high-resolution face images and we randomly split 29800 images for training and 200 images for testing. All images in both datasets are resized to  $256 \times 256$  as the input. For pre-training, we train the Transformer encoder and Transformer decoder using ImageNet-1K where the mask ratio is set to 75% for all images. Other training details, such as learning rate, optimizer, and weight decay are consistent with the setting in [23]. Then, the overall MCM is trained for 250K iterations on COCO and 90K iterations on CelebAMask-HQ. All the experiments are implemented on NVIDIA RTX 3090 GPUs.

### 4.2 Comparison with The State-of-the-Arts

We compare our MCM with recent state-of-the-art (SOTA) learned end-to-end image compression methods, including Xie *et al.* [53], Qian *et al.* [44], Bai *et al.* [1] and Chang *et al.* [14] as well as traditional image compression methods BPG [6] and VVC [8] on extremely low-bitrate conditions ( $< 0.1$ bpp). For a fair comparison, all the LIC methods are re-trained using their public source codes on the same datasets as ours. For BPG, we use the BPG software with YUV444 subsampling, x265 HEVC implementation, and 8-bit depth. For VVC, we use the VVC Official Test Model VTM 10.0 with an intra-profile configuration.

**Rate-distortion Performance.** Because the reconstructed images are heavily distorted at very low bitrates, pixel-level measurements such as classical PSNR and MS-SSIM can not well reflect the reconstruction quality. Therefore, in this work, we use Learned Perceptual Image Patch Similarity (LPIPS) [55] and Fréchet inception distance (FID) [25] which are widely used in image generation tasks [47, 15, 43], as the metrics to separately evaluate the perceptual quality of images and the distance of the original data and reconstructed data. Fig. 6 and Fig. 7 illustrate the Rate-LPIPS and Rate-FID on CelebAMask-HQ

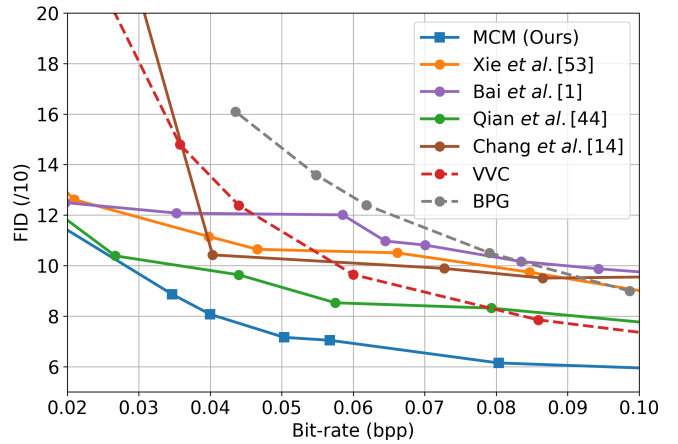
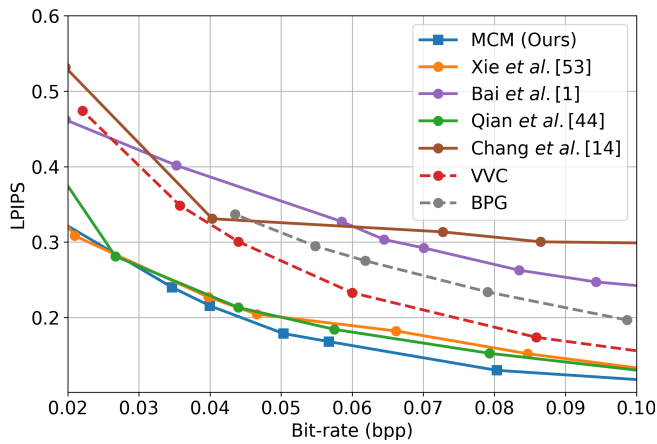


Fig. 6: The Rate-LPIPS and Rate-FID comparison on CelebAMask-HQ dataset.

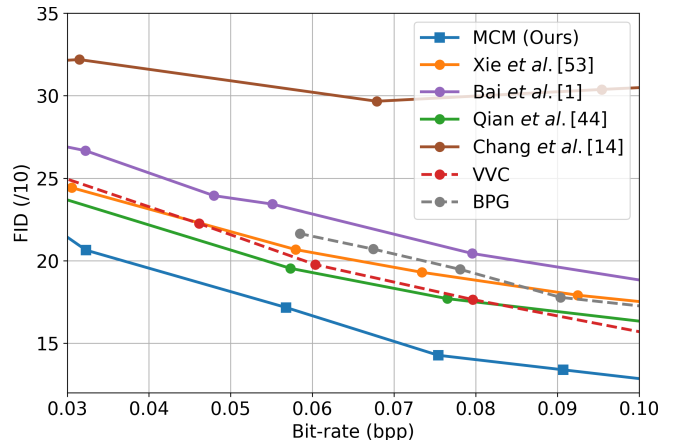
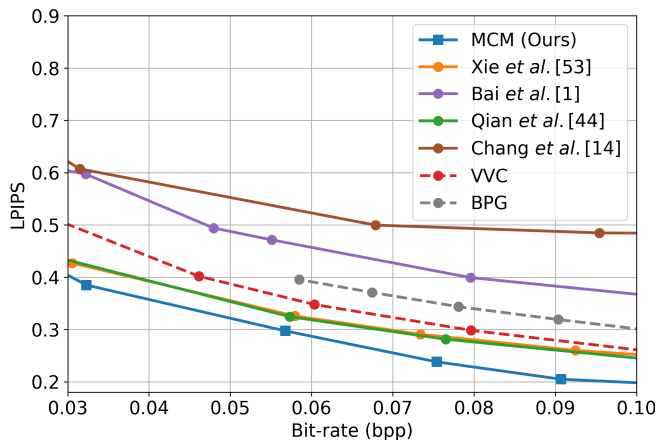


Fig. 7: The Rate-LPIPS and Rate-FID comparison on COCO dataset.

and COCO, respectively. Firstly, in Fig. 6, compared to existing LIC methods, classical coding standards BPG [6] and VVC [8] tend to perform better at higher bitrates (0.08-0.1bpp). Chang *et al.* [14] adopts a conceptual coding to compress structure and texture components individually for low bitrate, which shows worse R-D performance than other compared methods in terms of Rate-LPIPS but better than Xie *et al.* [53] and Bai *et al.* [1] on Rate-FID. Though Qian *et al.* [44] outperforms existing LIC methods and VVC [8] on both metrics, it is still inferior against our method at almost every R-D point. In Fig. 7, for the more challenging dataset COCO, we can see that the performance of Chang *et al.* [14] deteriorates heavily, no matter LPIPS or FID. By comparison, our method achieves the SOTA performance, which surpasses other methods by a large margin, especially on Rate-FID.

**Qualitative Comparison.** In Fig. 8, we illustrate the visual results of all methods for qualitative comparison. Generally, it can be observed our method can reconstruct the images with a more vivid texture

Table 1: Average BD-rate savings on COCO Dataset and CelebAMask-HQ Dataset. We adopt VVC as the anchor.

Method	COCO	CelebAMask-HQ
BPG	26.56%	26.39%
Bai <i>et al.</i> [1]	65.94%	33.50%
Chang <i>et al.</i> [14]	162.96%	1.23%
Qian <i>et al.</i> [44]	-20.16%	-38.68%
Xie <i>et al.</i> [53]	-18.51%	-35.96%
MCM (Ours)	<b>-30.81%</b>	<b>-41.97%</b>

appearance and global structural fidelity at low bitrates, while other methods produce results that suffer from more blurs and fewer local details with higher bitrates. As for CelebAMask-HQ, although all the compared methods show good visual quality, our results contain more details in the key facial components, such as the eyes and mouth.

**BD-rate savings.** Then, we quantify the R-D performance by evaluating the average BD-rate [7]

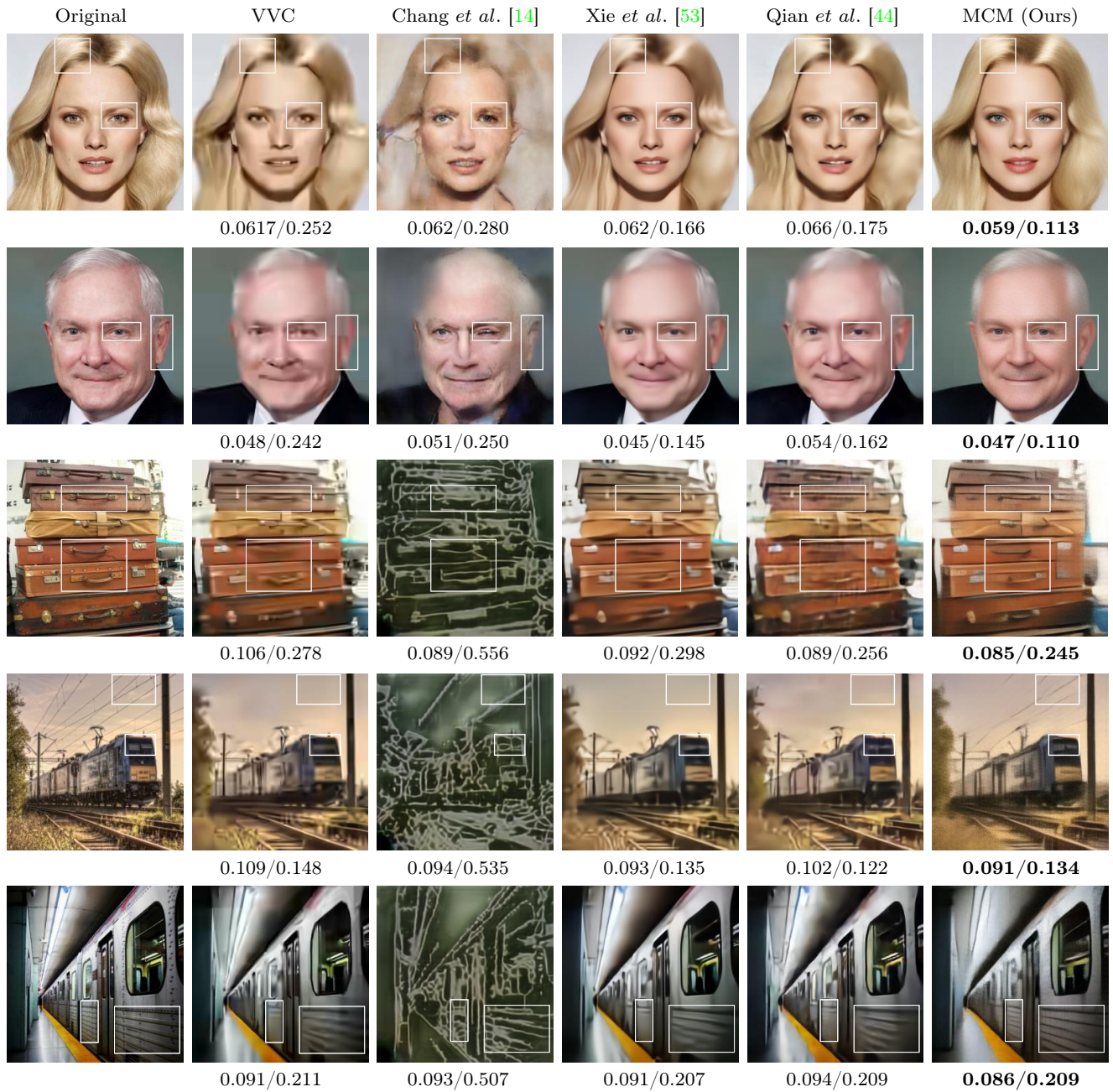


Fig. 8: Visual performance on CelebAMask-HQ and COCO dataset. Bpp $\downarrow$ /LPIPS $\downarrow$  of each method are also shown for comparison.

saving, which is calculated over the LPIPS results. Here, we use VVC as the anchor for comparison, where the results are shown in Table. 1. As we can see, Bai *et al.* [1] and Chang *et al.* [14] are less effective, which even require much more BD-rate than VVC (65.94% and 162.96% respectively). We can see that our MCM achieves 30.81% on COCO and 41.97% BD-rate savings on CelebAMask-HQ respectively, while that of the second-best approach Qian *et al.* [44] is only 20.16% on COCO and 38.68% on CelebAMask-HQ.

In general, our MCM achieves competitive bitrate cost while preserving superior reconstruction quality against existing SOTA image codecs.

**User Study.** We conduct a user study and investigate the human opinion of compressed images on all of the above methods. More specifically, we randomly select 100 images from the COCO and CelebAMask-HQ validation datasets respectively. We evaluate all the methods on two low bitrates, where 50 images are included at each bitrate. The reconstructed

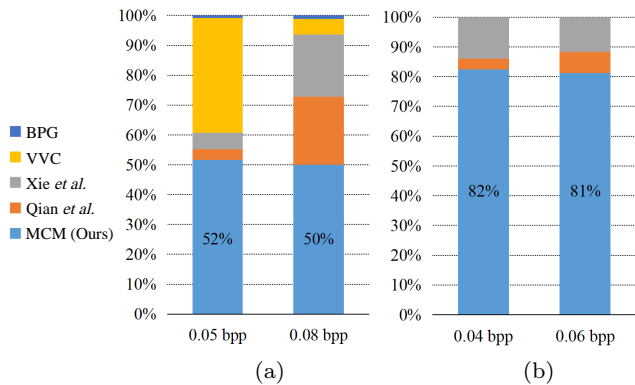


Fig. 9: The human opinion of various methods and ours on COCO (Fig(a)) and CelebAMask-HQ (Fig(b)) validation dataset.

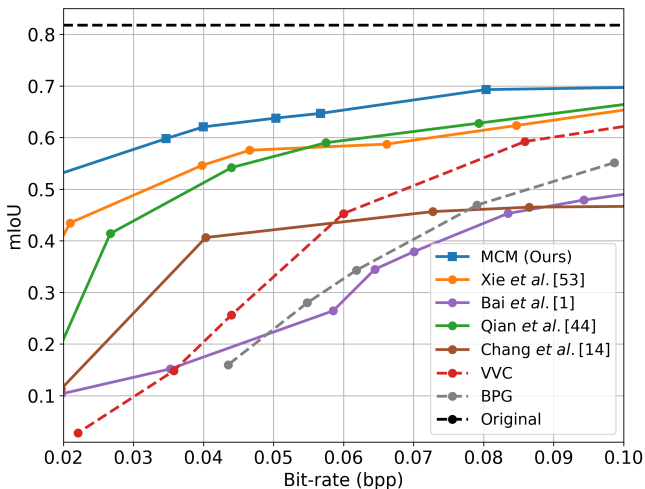


Fig. 10: Performance of face parsing on CelebAMask-HQ testset.

images under the same dataset and the same bitrate are assigned in a group. We invite 10 volunteers to pick up the best reconstruction according to the visual qualities from the group whose images are displayed in disorder. All user study is done under the same PC to avoid visual bias. As illustrated in Fig. 9, our MCM received the most votes on all datasets. There are more than 50% volunteers that appreciate our results at both bitrates on COCO, whereas BPG, VVC, Qian *et al.* [44] and Xie *et al.* [53] get 0.8%, 38.4%, 3.6%, 5.6% votes at 0.05bpp and 1.2%, 5.2%, 2.3%, 2.0% votes at 0.08bpp on COCO. Especially, our MCM gets a definite advantage on CelebAMask-HQ, obviously demonstrating its effectiveness.

### 4.3 Downstream Applications.

We further explore the effect of our MCM in downstream tasks using well-trained models on CelebAMask-HQ and utilize a popular face parsing method EHANet [40] as the backbone to conduct compression-based face parsing. Here, we apply mIoU (mean Intersection over Union) as the metric, where the original performance of EHANet on uncompressed images is adopted as a reference. As shown in Fig. 10, our MCM shows excellent performance under extremely low-bitrate compression conditions: about 10% mIoU drop down to 0.08bpp, and less than 15% mIoU drop down to 0.055bpp. Meanwhile, all compared methods lose over 15% mIoU already at 0.08bpp, while at 0.055bpp, they have lost about 20%-60% mIoU.

Moreover, in Fig. 11, we also visualize the instance segmentation results on COCO dataset to validate the impact of MCM. We adopt pre-trained Mask R-CNN [24] as the segmentor and feed the compressed images into it to obtain the segmentation results. Besides the ground truth segmentation map, the results on original uncompressed images are used for reference. As shown in Fig. 11, in the simple example (1st row), our MCM successfully segments all the objects with better boundaries and the fewest bitrate cost. Even on images with more complex scenes and objects (last two rows), MCM still achieves more accurate segmentation performance while maintaining competitive efficiency. More surprisingly, the reference results show mislabelling of a bench in the 2nd example and overlapped persons in the 3rd example.

### 4.4 Ablation Study.

**Effect of DA-Mask.** In order to explore the effectiveness of our proposed DA-Mask strategy, we first construct three variants: 1) Random masking; 2) Texture-guided masking only, and 3) Structure-guided masking only, to make a comparison. It should be noted that all the variants are compared under the same masking ratio. As shown in Table 2, the model with random masking involves the lowest bitrate but the worst LPIPS performance. When we replace the random masking with texture-guided strategy, the model performs slightly better than that with structure-guided masking but costs more bitrates. This is because the former focuses on the textures over the entire image while the latter only focuses on the semantic structure of the visual object. This is more pronounced on CelebAMask-HQ, in which the structural semantics in facial images are mainly described by key parts and outlines of the face,

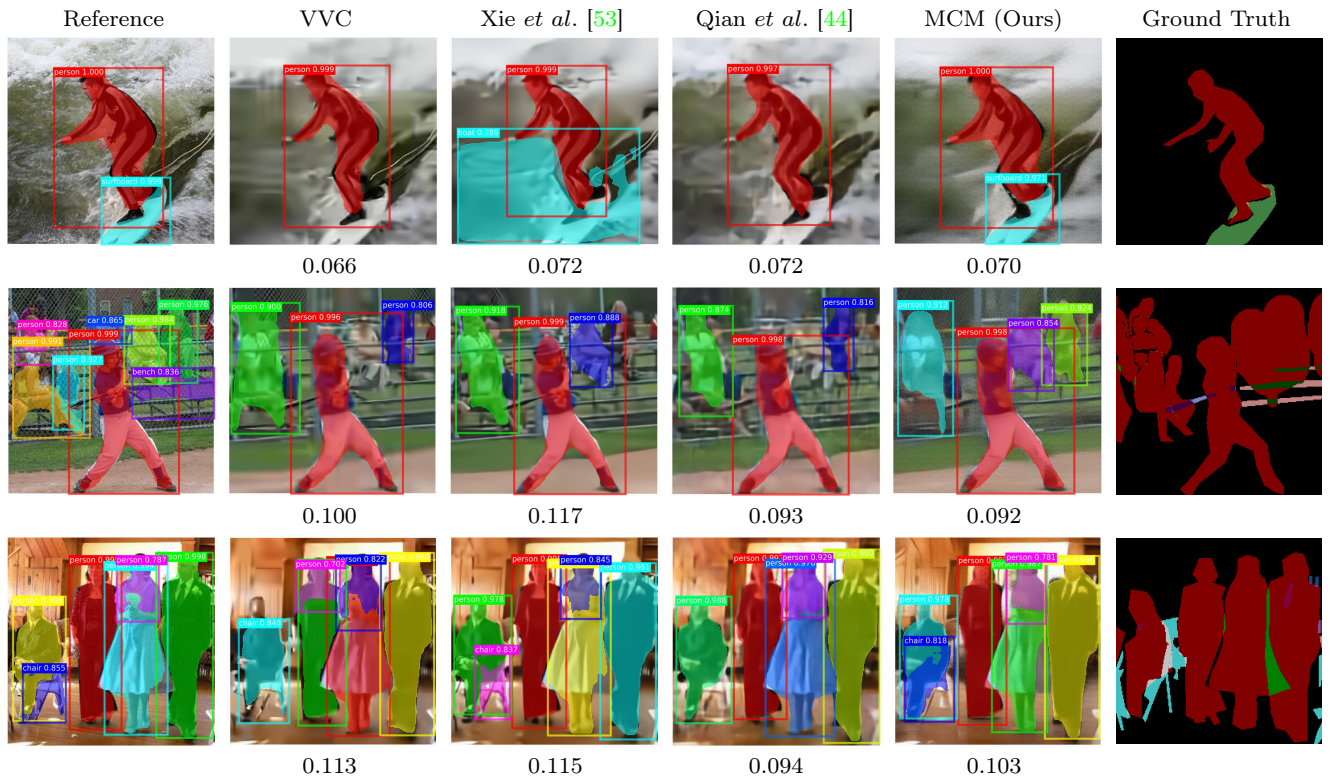


Fig. 11: Visual performance of instance segmentation on COCO dataset. The bitrate (bpp) of each method is also shown for comparison.

Table 2: Quantitative comparison on COCO and CelebAMask-HQ datasets between the models with different masking strategies.

Dataset	Sampling Strategy	Average bitrate↓	LPIPS↓
COCO	Random	0.0723	0.263
	Texture	0.0760	0.230
	Structure	0.0737	0.257
	DA-Mask	<b>0.0754</b>	<b>0.238</b>
CelebAMask-HQ	Random	0.0839	0.147
	Texture	0.0885	0.117
	Structure	0.0776	0.199
	DA-Mask	<b>0.0803</b>	<b>0.130</b>

such as eyes and mouth, *etc.*, thus enabling lower bitrates than other methods. Our DA-Mask samples the patches based on the texture and structure complexity to balance the local texture and structural semantics, which achieves a good trade-off between bitrate consumption and perceptual quality. To more intuitively validate the influence of different masking strategies for image compression, we illustrate their corresponding visual results in Fig. 12. As we can see, the model with random masking shows a good reconstruction effect but fails to recover the local details (Fig. 12 (a)). Though using only texture-guided masking can make an improvement, it tends to ignore some semantic objects (Fig. 12 (b)). In contrast, the

structure-guided approach is able to retain semantic-related patches. However, it discards too many textures (Fig. 12 (c)). By comparison, our DA-Mask can facilitate the model to simultaneously pay attention to important texture and semantic information of images (Fig. 12 (d)), which produces more plausible images.

**Study of Masking ratio.** In this subsection, we investigate the impact of the masking ratio setting in MCM. Given a  $256 \times 256$  image, we divide it into 256 patches of the size  $16 \times 16$ . The number of visible patches is set to 144 and 64, whose corresponding masking ratios are 43% and 75%, respectively. Fig. 13 shows the masked input and reconstructed output with the above two masking ratios, in which the

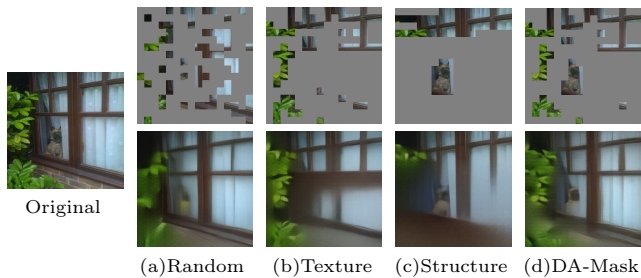


Fig. 12: Visual comparison of four mask sampling strategies.

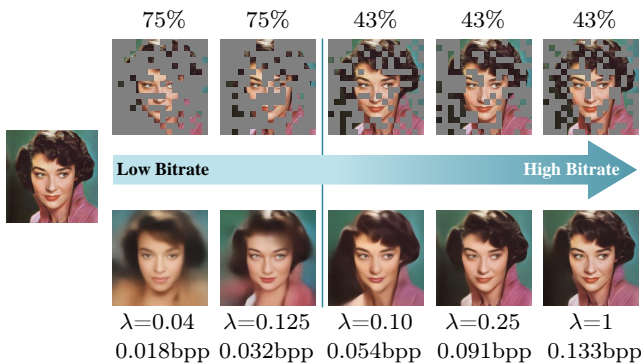


Fig. 13: Impact of different masking ratio settings for image compression. From left to right, we set such values as 43% and 75% to select visible patches respectively. At the same masking ratio, we control the  $\lambda$  in R-D loss.

former two images are 75% masked and the latter three images are 43% masked. Besides, at the same masking ratio, we control the Lagrange multiplier  $\lambda$  in R-D loss (shown in Eq. (10)) to adjust the bitrates. Obviously, the masking ratio plays a deterministic role in both bitrate and image quality. We can find the higher ratio the more information losses, resulting in lower bitrates and poorer reconstruction quality (2nd column *v.s.* 3rd column). Besides, by combining DA-Mask and the LIC module, we can jointly optimize the overall network and continuously increase the  $\lambda$  values to realize quality enhancement at higher bitrates, ultimately achieving effective reconstruction while still maintaining extremely low bitrate compression (last column).

## 5 Conclusion

In this work, we have proposed a novel masked compression model (MCM) which combines the merits of pre-trained masked autoencoder (MAE) and learned image compression (LIC) for extremely low-bitrate image compression. Specifically, we present a dual-

adaptive masking (DA-Mask) strategy which performs probability patch sampling based on image structure and texture distributions. This approach enables the model to adaptively sample informative patches that are conducive to image reconstruction while achieving effective redundancy removal. We note that DA-Mask with pre-trained MAE can well cooperate with LIC to learn meaningful semantic context and texture representations for effective and efficient image compression. Experimental results show that at extremely low bitrates, our MCM is superior to existing classical standard codecs and LIC methods in terms of R-D performance, human perception, and bitrate savings, and also shows better transferability to downstream tasks.

## References

- Bai, Y., Yang, X., Liu, X., Jiang, J., Wang, Y., Ji, X., Gao, W.: Towards end-to-end image compression and analysis with transformers. In: Proceedings of the AAAI Conference on Artificial Intelligence, vol. 36, pp. 104–112 (2022)
- Ballé, J., Laparra, V., Simoncelli, E.P.: End-to-end optimized image compression. In: International Conference on Learning Representations (2017)
- Ballé, J., Laparra, V., Simoncelli, E.P.: End-to-end optimized image compression. In: International Conference on Learning Representations (2017)
- Ballé, J., Minnen, D., Singh, S., Hwang, S.J., Johnston, N.: Variational image compression with a scale hyperprior. arXiv preprint arXiv:1802.01436 (2018)
- Bao, H., Dong, L., Piao, S., Wei, F.: Beit: Bert pre-training of image transformers. arXiv preprint arXiv:2106.08254 (2021)
- Bellard, F.: Bpg image format. URL <https://bellard.org/bpg> (2015)
- Bjontegaard, G.: Calculation of average psnr differences between rd-curves. ITU SG16 Doc. VCEG-M33 (2001)
- Bross, B., Chen, J., Ohm, J.R., Sullivan, G.J., Wang, Y.K.: Developments in international video coding standardization after avc, with an overview of versatile video coding (vvc). Proceedings of the IEEE **109**(9), 1463–1493 (2021)
- Brown, T., Mann, B., Ryder, e.a.: Language models are few-shot learners. In: H. Larochelle, M. Ranzato, R. Hadsell, M. Balcan, H. Lin (eds.) Advances in Neural Information Processing Systems, vol. 33, pp. 1877–1901 (2020)
- Cai, J., Cao, Z., Zhang, L.: Learning a single tucker decomposition network for lossy image compression with multiple bitsperpixel rates. IEEE Transactions on Image Processing **29**, 3612–3625 (2018)
- Carion, N., Massa, F., Synnaeve, G., Usunier, N., Kirillov, A., Zagoruyko, S.: End-to-end object detection with transformers. In: Computer Vision–ECCV 2020: 16th European Conference, Glasgow, UK, August 23–28, 2020, Proceedings, Part I 16, pp. 213–229. Springer (2020)
- Chang, H., Zhang, H., Jiang, L., Liu, C., Freeman, W.T.: Maskgit: Masked generative image transformer. In:

- The IEEE Conference on Computer Vision and Pattern Recognition (2022)
13. Chang, J., Zhang, J., Xu, Y., Li, J., Ma, S., Gao, W.: Consistency-contrast learning for conceptual coding. In: Proceedings of the 30th ACM International Conference on Multimedia, pp. 2681–2690 (2022)
  14. Chang, J., Zhao, Z., Jia, C., Wang, S., Yang, L., Mao, Q., Zhang, J., Ma, S.: Conceptual compression via deep structure and texture synthesis. *IEEE Transactions on Image Processing* **31**, 2809–2823 (2022)
  15. Chang, Y.L., Liu, Z.Y., Lee, K.Y., Hsu, W.: Free-form video inpainting with 3d gated convolution and temporal patchgan. In: Proceedings of the IEEE/CVF International Conference on Computer Vision, pp. 9066–9075 (2019)
  16. Chen, H., Wang, Y., Guo, T., Xu, C., Deng, Y., Liu, Z., Ma, S., Xu, C., Xu, C., Gao, W.: Pre-trained image processing transformer. In: Proceedings of the IEEE/CVF Conference on Computer Vision and Pattern Recognition, pp. 12299–12310 (2021)
  17. Cheng, Z., Sun, H., Takeuchi, M., Katto, J.: Learning image and video compression through spatial-temporal energy compaction. In: Proceedings of the IEEE/CVF Conference on Computer Vision and Pattern Recognition, pp. 10071–10080 (2019)
  18. Dash, S., Kumaravelu, G., Naganoor, V., Raman, S.K., Ramesh, A., Lee, H.: Compressnet: Generative compression at extremely low bitrates. In: 2020 IEEE Winter Conference on Applications of Computer Vision, pp. 2314–2322 (2020)
  19. Devlin, J., Chang, M.W., Lee, K., Toutanova, K.: Bert: Pre-training of deep bidirectional transformers for language understanding. *arXiv preprint arXiv:1810.04805* (2018)
  20. Dinh, L., Krueger, D., Bengio, Y.: NICE: non-linear independent components estimation. In: In Proceedings of the International Conference on Learning Representations Workshops (2015)
  21. Duan, H., Shen, W., Min, X., Tu, D., Teng, L., Wang, J., Zhai, G.: Masked autoencoders as image processors (2023)
  22. Gao, P., Ma, T., Li, H., Lin, Z., Dai, J., Qiao, Y.: MCMAE: Masked convolution meets masked autoencoders. In: Advances in Neural Information Processing Systems (2022)
  23. He, K., Chen, X., Xie, S., Li, Y., Doll’ar, P., Girshick, R.B.: Masked autoencoders are scalable vision learners. 2022 IEEE/CVF Conference on Computer Vision and Pattern Recognition pp. 15979–15988 (2021)
  24. He, K., Gkioxari, G., Dollár, P., Girshick, R.: Mask r-cnn. In: Proceedings of the IEEE international conference on computer vision, pp. 2961–2969 (2017)
  25. Heusel, M., Ramsauer, H., Unterthiner, T., Nessler, B., Hochreiter, S.: Gans trained by a two time-scale update rule converge to a local nash equilibrium. *Advances in neural information processing systems* **30** (2017)
  26. Huang, L., You, S., Zheng, M., Wang, F., Qian, C., Yamasaki, T.: Green hierarchical vision transformer for masked image modeling. Thirty-Sixth Conference on Neural Information Processing Systems (2022)
  27. Huang, Z., Jin, X., Lu, C., Hou, Q., Cheng, M.M., Fu, D., Shen, X., Feng, J.: Contrastive masked autoencoders are stronger vision learners. *arXiv preprint arXiv:2207.13532* (2022)
  28. Huffman, D.A.: A method for the construction of minimum-redundancy codes. *Proceedings of the IRE* **40**(9), 1098–1101 (1952)
  29. Jang, E., Gu, S., Poole, B.: Categorical reparameterization with gumbel-softmax. In: International Conference on Learning Representations (2017)
  30. Jiang, F., Tao, W., Liu, S., Ren, J., Guo, X., Zhao, D.: An endtoend compression framework based on convolutional neural networks. *IEEE Transactions on Circuits and Systems for Video Technology* **28**(10), 3007–3018 (2017)
  31. Johnson, J., Alahi, A., Fei-Fei, L.: Perceptual losses for real-time style transfer and super-resolution. In: Computer Vision–ECCV 2016: 14th European Conference, Amsterdam, The Netherlands, October 11–14, 2016, Proceedings, Part II 14, pp. 694–711. Springer (2016)
  32. Kolesnikov, A., Dosovitskiy, A., Weissenborn, D., Heigold, G., Uszkoreit, J., Beyer, L., Minderer, M., Dehghani, M., Hounsby, N., Gelly, S., Unterthiner, T., Zhai, X.: An image is worth 16x16 words: Transformers for image recognition at scale (2021)
  33. Lee, C.H., Liu, Z., Wu, L., Luo, P.: Maskgan: Towards diverse and interactive facial image manipulation. In: Proceedings of the IEEE/CVF Conference on Computer Vision and Pattern Recognition, pp. 5549–5558 (2020)
  34. Lee, J., Cho, S., Beack, S.K.: Contextadaptive entropy model for end-to-end optimized image compression. In: International Conference on Learning Representations (2019)
  35. Lezama, J., Chang, H., Jiang, L., Essa, I.: Improved masked image generation with token-critic. In: Computer Vision–ECCV 2022: 17th European Conference, Tel Aviv, Israel, October 23–27, 2022, Proceedings, Part XXIII, pp. 70–86. Springer (2022)
  36. Li, M., Zuo, W., Gu, S., Zhao, D., Zhang, D.: Learning convolutional networks for content-weighted image compression. In: Proceedings of the IEEE/CVF Conference on Computer Vision and Pattern Recognition, pp. 3214–3223 (2018)
  37. Li, T., Chang, H., Mishra, S.K., Zhang, H., Katabi, D., Krishnan, D.: Mage: Masked generative encoder to unify representation learning and image synthesis (2022)
  38. Lin, T.Y., Maire, M., Belongie, S., Hays, J., Perona, P., Ramanan, D., Dollár, P., Zitnick, C.L.: Microsoft coco: Common objects in context. In: Computer Vision–ECCV 2014: 13th European Conference, Zurich, Switzerland, September 6–12, 2014, Proceedings, Part V 13, pp. 740–755. Springer (2014)
  39. Liu, Z., Lin, Y., Cao, Y., Hu, H., Wei, Y., Zhang, Z., Lin, S., Guo, B.: Swin transformer: Hierarchical vision transformer using shifted windows. In: Proceedings of the IEEE/CVF Conference on Computer Vision and Pattern Recognition, pp. 10012–10022 (2021)
  40. Luo, L., Xue, D., Feng, X.: Ehanet: An effective hierarchical aggregation network for face parsing. *Applied Sciences* **10**(9), 3135 (2020)
  41. Minnen, D., Ballé, J., Toderici, G.D.: Joint autoregressive and hierarchical priors for learned image compression. *Advances in neural information processing systems* **31** (2018)
  42. Minnen, D., Singh, S.: Channelwise autoregressive entropy models for learned image compression. In: 2020 IEEE International Conference on Image Processing, pp. 3339–3343. IEEE (2020)
  43. Nazeri, K., Ng, E., Joseph, T., Qureshi, F., Ebrahimi, M.: Edgeconnect: Structure guided image inpainting using edge prediction. In: 2019 IEEE/CVF International Conference on Computer Vision Workshop, pp. 3265–3274 (2019)

44. Qian, Y., Lin, M., Sun, X., Tan, Z., Jin, R.: Entroformer: A transformer-based entropy model for learned image compression. In: International Conference on Learning Representations (2022)
45. Radford, A., Narasimhan, K.: Improving language understanding by generative pre-training (2018)
46. Radford, A., Wu, J., Child, R., Luan, D., Amodei, D., Sutskever, I.: Language models are unsupervised multitask learners (2019)
47. Rombach, R., Blattmann, A., Lorenz, D., Esser, P., Ommer, B.: High-resolution image synthesis with latent diffusion models. In: Proceedings of the IEEE/CVF Conference on Computer Vision and Pattern Recognition, pp. 10684–10695 (2022)
48. Santurkar, S., Budden, D., Shavit, N.: Generative compression. In: 2018 Picture Coding Symposium, pp. 258–262 (2018)
49. Sun, J., Xu, Z., Shum, H.Y.: Image super-resolution using gradient profile prior. In: 2008 IEEE Conference on Computer Vision and Pattern Recognition, pp. 1–8 (2008)
50. Taubman, D.S., Marcellin, M.W., Rabbani, M.: Jpeg2000: Image compression fundamentals, standards and practice. *Journal of Electronic Imaging* **11**(2), 286–287 (2002)
51. Wallace, G.K.: Overview of the jpeg (isocitt) still image compression standard. In: Image Processing Algorithms and Techniques, vol. 1244, pp. 220–233. SPIE (1990)
52. Wang, Z., Bovik, A.C., Sheikh, H.R., Simoncelli, E.P.: Image quality assessment: from error visibility to structural similarity. *IEEE transactions on image processing* **13**(4), 600–612 (2004)
53. Xie, Y., Cheng, K.L., Chen, Q.: Enhanced invertible encoding for learned image compression. In: Proceedings of the ACM International Conference on Multimedia, pp. 162–170 (2021)
54. Xie, Z., Zhang, Z., Cao, Y., Lin, Y., Bao, J., Yao, Z., Dai, Q., Hu, H.: Simsim: a simple framework for masked image modeling. In: 2022 IEEE/CVF Conference on Computer Vision and Pattern Recognition, pp. 9643–9653 (2022)
55. Zhang, R., Isola, P., Efros, A.A., Shechtman, E., Wang, O.: The unreasonable effectiveness of deep features as a perceptual metric. In: Proceedings of the IEEE/CVF Conference on Computer Vision and Pattern Recognition, pp. 586–595 (2018)
56. Zheng, S., Lu, J., Zhao, H., Zhu, X., Luo, Z., Wang, Y., Fu, Y., Feng, J., Xiang, T., Torr, P.H., et al.: Rethinking semantic segmentation from a sequence-to-sequence perspective with transformers. In: Proceedings of the IEEE/CVF Conference on Computer Vision and Pattern Recognition, pp. 6881–6890 (2021)
57. Zhu, X., Song, J., Gao, L., Zheng, F., Shen, H.T.: Unified multivariate gaussian mixture for efficient neural image compression. In: Proceedings of the IEEE/CVF Conference on Computer Vision and Pattern Recognition, pp. 17612–17621 (2022)
58. Zou, R., Song, C., Zhang, Z.: The devil is in the details: Window-based attention for image compression. In: Proceedings of the IEEE/CVF Conference on Computer Vision and Pattern Recognition, pp. 17492–17501 (2022)